Experimental and Theoretical Study of the Secondary Equilibrium Isotope Effect (SEIE) in the Proton Transfer between the Pyridinium-d5Cation and Pyridine†

ARTICLE *in* THE JOURNAL OF PHYSICAL CHEMISTRY A · AUGUST 2003

Impact Factor: 2.69 · DOI: 10.1021/jp035109i

Experimental and Theoretical Study of the Secondary Equilibrium Isotope Effect (SEIE) in the Proton Transfer between the Pyridinium-d_5 Cation and Pyridine†

C. Muñoz-Caro* and A. Niño

Grupo de Química Computacional, Escuela Superior de Informática, Universidad de Castilla-La Mancha, Paseo de la Universidad 4, 13071 Ciudad Real, Spain

J. Z. Dávalos, E. Quintanilla, and J. L. Abboud

Instituto de Química Física "Rocasolano", Consejo Superior de Investigaciones Científicas, Serrano 119, 28006 Madrid, Spain

Received: April 24, 2003; In Final Form: June 18, 2003

In this work we present an experimental and theoretical study of the proton transfer from the pyridinium-d_5 cation to pyridine. FT-ICR measurements yield, at 331 K, an equilibrium constant $K = 0.809$ ($\Delta_r G^\circ_m = 0.58$ kJ mol^{-1}) for the process, favoring the pyridine form. The structural and bonding changes on protonation of pyridine are analyzed by applying the atoms in molecules theory. As a consequence of electronic density redistribution, we found that on protonation the CN and the CC bonds placed farther from the nitrogen weaken. In addition, the CH and the CC bonds closer to the nitrogen increase their strength. Thermostatistical computation of the equilibrium constant from data obtained at the B3LYP/cc-pVTZ level, within the harmonic approximation, predicts a value of 0.827 ($\Delta_r G^\circ_m$ value of 0.52 kJ mol^{-1}), in good agreement with the 0.809 ± 0.027 experimental result for a 99.9% confidence level. A simple statistical mechanical model intended to apply under conditions close to the present ones is developed. The model allows for a fine-tuning of the thermodynamic state functions for the equilibrium. This model shows that rather than by translational and rotational variations, the reaction is driven by the changes in zero point energies and in the density of vibrational states. In addition, theoretical analysis of the enthalpic and entropic contributions shows that the $\Delta_r G^\circ_m$ value is determined by the enthalpic part. It is also predicted that the $\Delta_r G^\circ_m$ value decreases with temperature. We found that this effect is due to a higher density of vibrational states in the pyridine-d_5 form. A new model is developed to correct the vibrational partition function for anharmonicity. This model shows that correction for anharmonicity in the low-frequency modes reduces significantly the difference between calculated and experimental K values.

Introduction

The term isotope effect refers to the change in chemical or physical properties between chemical species differing in their isotopic composition. Thus, it is the simplest substitution that we can make in a compound. Despite its simplicity, isotopic substitution has a clear and observable effect in the molecular properties. With respect to a chemical reaction, this effect can be observed in equilibrium conditions, the equilibrium isotope effect (EIE), or in the kinetics of the reaction, the kinetic isotope effect (KIE). The first one is measured as the ratio of equilibrium constants (with and without isotopic substitution), whereas the second is defined as the ratio of rate constants. In this context, isotope effects are further classified as primary or secondary. In primary isotope effects (PIE), the bonds broken or formed in the reaction involve the isotopic species. Thus, especially for the pair hydrogen/deuterium, the PIE is clear, corresponding to a few percent of the observed property.[1] On the other hand, in secondary isotope effects (SIE) the isotopic substituted atoms are not involved in the breaking of forming of bonds. Therefore, the SIE has a much smaller effect in the reaction than does PIE.[2]

Within the framework of the Born−Oppenheimer approximation, isotopic substitution does not modify the potential energy hypersurface of the system. The effect of the isotopic substitution on a chemical system can be accounted for in terms of the variation of masses. Thus, it is the change in the translational, rotational, and especially, vibrational behavior that determines the difference in properties. Therefore, the thermostatistical determination of the equilibrium constant is the basis for the treatment of EIE. A similar treatment, within the transition state theory, represents the basis for the KIE. With simplified assumptions, the classical Bigeleisen treatment of the isotope effect is performed in this way.[3]

The first experimental proof of a kinetic isotope effect dates back to the discovery in 1932 by Washburn and Urey that deuterium is enriched in the liquid phase in the electrolysis of water.[4] Isotope effects can be very large, as for instance the secondary EIE for the reduction of aromatic hydrocarbons to their radical anions.[5] In this context, theoretical treatments are found invaluable in the rationale of these phenomena.[6] Isotope effects have also been observed in such reactions as H-atom transfer and H_2-molecule elimination.[7] With respect to these cases, the isotope effects in tunneling are pronounced, because the difference in mass is important, such as in the hydrogen/deuterium couple. In some problems of this kind, the variational

† This work is dedicated to the memory of Dr. V. Botella.

* Corresponding author. Fax: 34-926-295354. E-mail: quimcom@uclm.es.

10.1021/jp035109i CCC: $25.00
Published on Web 07/23/2003

transition state theory and the multidimensional semiclassical tunneling method have been useful.[8] Large KIE have also experimentally detected for the couple $^{12}C/^{13}C$ in the reaction of methane with chlorine atoms,[9] which is so important in the chemistry of the atmosphere.

In this work we present the experimental determination and the theoretical treatment of the secondary equilibrium isotope effect (SEIE) for the proton transfer between the pyridinium-d_5 cation and pyridine. Thus, the different molecular species involved are structurally characterized. In addition, the bonding changes of pyridine on protonation are also taken into account. The Gibbs energy variation, $\Delta_r G^\circ_m$, is measured by Fourier Transform Ion Cyclotron Resonance (FT-ICR) spectroscopy. $\Delta_r G^\circ_m$ is also thermostatistically determined and analyzed. The variation of the equilibrium constant with the temperature is determined, as well as the enthalpic and entropic contributions. Finally, the effect of anharmonicity on the computed thermodynamic values is also taken into account. The small magnitude of the equilibrium constant makes this problem an interesting test case to determine the suitability of present theoretical tools to describe and interpret small physical effects.

Experimental Section

A. FT ICR Spectrometer. The study was performed on a modified Bruker CMS-47 FT-ICR mass spectrometer[10] already used in previous studies,[11] and the spectra were acquired using an IonSpec Omega Data Station. (IonSpec, Irvine, CA). The high field strength of the superconducting magnet (4.7 T) easily allows the monitoring of the ion−molecule reaction for relatively long reaction times.

B. Reagents. Pyridine (Py, purity >99.9%), pyridine-d_5 (Py-d_5, isotopic purity >99.6%), and H_2S (purity >99.5%) were purchased from Aldrich and used without further purification. No impurities were detected in the experiments.

C. Sample Preparation. Mixtures of both pyridines (Py and Py-d_5), covering the range of molar ratios (n_{Py-d_5}/n_{Py}) 0.1450−0.36451, were prepared by weight. Typically, samples of these compounds (masses in the range 5−20 mg) were enclosed and sealed under nitrogen in separated thin-walled glass ampules. Masses were determined within ±2 μg using a Mettler AT-21 microbalance. The ampules were introduced into a 1-L glass balloon, and the system was degassed for several hours down to pressures of ca. 10^{-7} mbar. At this point, degassing was stopped and the ampules broken. After 1 h, the gaseous mixture was allowed to enter the high-vacuum section of the spectrometer.

D. Experimental Conditions. The temperature of the cell was 331 ± 2 K as determined using a calibrated platinum thermometer (platinum resistor) located close to one of the repeller plates of the ICR cell. The experimental setup was similar to the one described by Fridgen et al.[12] Nominal total pressures of the mixtures of pyridines were in the $(0.5-5) \times 10^{-8}$ mbar range, as indicated by the Bayard-Alpert ionization gauge (Balzers IMR-132). H_2S was added up to nominal pressures of $(3-4) \times 10^{-7}$ mbar. Electron ionization of H_2S was carried out using nominal energies of 11−12 eV. Under these conditions, H_3S^+ was readily generated and used as a clean proton source. H_2S also plays the role of a thermal bath.

When necessary, ion selection was achieved using both broadband elimination and single shots.

Theory

Because the measurements are made in a vacuum, we use electronic structure methods to represent the molecular systems in its (lack of) environment. Thus, we use the correlation consistent triple-ζ plus polarization basis set, cc-pVTZ. This basis includes as polarization functions, up to d functions on hydrogens and up to f functions on heavy atoms.[13] Correlation energy is accounted for by means of density functional theory. Thus, we use the Becke's three-parameter hybrid functional, with gradient corrections provided by the LYP correlation functional: B3LYP.[14] The three parameters of the B3LYP method are adjusted to reproduce the equilibrium data of the G1 molecule set.[15] Thus, although the DFT methology only partially accounts for the correlation energy, the results for equilibrium properties can be expected to be very reliable, as we have previously discussed.[16] Also, this basis has been tested by Szafran and Koput in neutral pyridine and its isotopomers, obtaining good agreement with experimental data for geometry, dipole moment, and frequencies.[17] All the electronic structure calculations have been carried out with the Gaussian 98 package.[18] The atoms in molecules theory is applied with the Morphy 98 program.[19] Thermodynamic properties are determined statistically from the geometry and harmonic frequencies computed at the fully relaxed structures. Thermodynamic properties and decomposition of the partition functions are obtained by means of the PARTI program.[20]

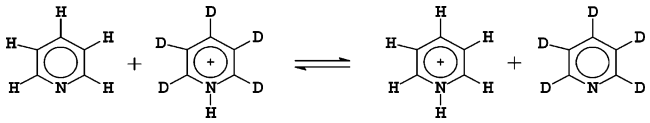

Figure 1. Equilibrium for the proton transfer between the pyridinium-d_5 cation and pyridine.

Results and Discussion

The equilibrium reaction for the proton-transfer process is shown in Figure 1. As written, we have four species; pyridine (Py) plus pyridinium-d_5 ((Py-d_5)−H^+) cation, to yield pyridinium cation (Py−H^+) plus pyridine-d_5 (Py-d_5). From the experimental standpoint, the key problem is the accurate determination of the dimensionless equilibrium constant K for reaction 1, defined through eq 2.

$$\mathrm{Py} + (\mathrm{Py}\text{-}d_5)\text{−}\mathrm{H}^+ \leftrightarrows \mathrm{Py}\text{−}\mathrm{H}^+ + \mathrm{Py}\text{-}d_5 \qquad (1)$$

$$K = [(P_{\mathrm{Py-H^+}}/P_{(\mathrm{Py}-d_5)-\mathrm{H}^+})][P_{(\mathrm{Py}-d_5)}/P_{\mathrm{Py}}] \qquad (2)$$

The ratio of the partial pressures of the neutral species, P_{Py-d_5}/P_{Py}, is given by their molar ratio, n_{Py-d_5}/n_{Py}. The latter is known to better than 4×10^{-4} by using gaseous mixtures of the neutral species prepared by weight (see Experimental Section). The ratio of the partial pressures of the ions Py−H^+ (m/z = 80 Da) to (Py-d_5)−H^+ (m/z = 85 Da), $P_{Py-H^+}/P_{(Py-d_5)-H^+}$, is taken as the ratio of their relative intensities, I_{80}/I_{85}, as determined by Fourier transform ion cyclotron spectroscopy (FT ICR).[21] ICR has long been used for the purpose of measuring kinetic[22] and thermodynamic[23] isotope effects in ion−molecule reactions.

Although full details are given in the Experimental Section, here we mention the main features of the experiments.

Mixtures of Py-d_5, Py, and a large excess of H_2S are subject to electron ionization. The main processes initially taking place are thus reactions 3a and 3b. H_3S^+(g) is then isolated using

$$H_2S(g) \rightarrow H_2S^{\bullet+}(g) + e^-(g) \qquad (3a)$$

$$H_2S^{\bullet+}(g) + H_2S(g) + \rightarrow HS^{\bullet}(g) + H_3S^{\bullet+}(g) \qquad (3b)$$

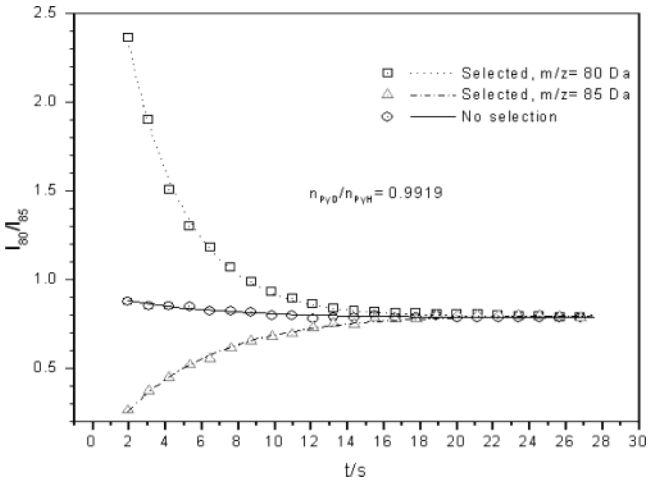

Figure 2. Example result of the experimental (I_{80}/I_{85}) ratio evolution.

TABLE 1: Experimental determinination of the equilibrium constant, *K*, for reaction 1 at 331 ± 2 K

n_{Py-d5}/n_{Py}	$K_{selected80}$[a]	$K_{selected85}$[a]	$K_{noselection}$[a]
0.1450	0.7606	0.7480	0.7474
0.3036	0.8283	0.8098	0.8045
0.3036	0.8231	0.8324	0.8091
0.3320	0.7730	0.7534	0.7438
0.9919	0.7812	0.8350	0.8281
0.9919	0.8287	0.8825	0.8367
1.8637	0.7534	0.7966	0.7330
2.1794	0.8474	0.8445	0.8488
3.6451	0.7867	0.8250	0.7647

av value, $K = 0.809$; sd=0.040

[a] Defined in the text.

ion-selection techniques and allowed to protonate Py(g) and Py-d_5(g). H_3S^+(g) is a clean proton source inasmuch as the gas-phase basicity[24] of H_2S (673.8 kJ mol^{-1})[25] is 224.3 kJ mol^{-1} lower than that of Py (898.1 kJ mol^{-1}).[25] The low hydrogen-bonding basicity of H_2S is most valuable because, even in the presence of relatively high pressures of this compound, the formation of species such as Py$-H^+\cdots SH_2$ is not observed. Reaction 1 is then monitored for periods of time of up to 120 s. The evolution of the ratio (I_{80}/I_{85}) is examined under three different experimental conditions: (i) free evolution, (ii) selection of (Py-d_5)$-H^+$, (iii) selection of Py$-H^+$. An example of such a study is presented in Figure 2.

It is clear that equilibrium (1) is reached in all three cases. Furthermore, these experiments provide limiting values of the ratio (I_{80}/I_{85}), which agree with a standard deviation of 5%. The experimental database is presented in Table 1, where as can be seen, the ratio (n_{Py-d_5}/n_{Py}) was varied by a factor of 25 and some experiments were repeated using the same ratio (n_{Py-d_5}/n_{Py}) and different total pressures.

The average value of *K* derived therefrom equals 0.809 with a confidence interval of 0.027 at the 99.9% confidence level[26] at 331 ± 2 K.

Because the experimental data are obtained in a vacuum at a very small pressure, we can use the ideal gas model as a good approximation. Thus, the statistical expressions for *H*, *S*, and *G* for our species are given by

$$H = kT^2(\partial \ln Q/\partial T)_V + kTV(\partial \ln Q/\partial V)_T$$

$$S = kT(\partial \ln Q/\partial T)_V + k \ln Q$$

$$G = -kT \ln Q + kTV(\partial \ln Q/\partial V)_T \qquad (4)$$

where the canonical partition function is obtained as $Q = q^N/N!$, in terms of the molecular partition function, *q*. In addition, and taking into account that the potential energy hypersurface is the same for the couples (Py, Py-d_5) and (Py$-H^+$, (Py-d_5)$-H^+$), the statistical expression for the equilibrium constant adopts the simple form

$$K = [q(\text{Py-}d_5)\cdot q(\text{Py}-H^+)]/[q(\text{Py})\cdot q((\text{Py-}d_5)-H^+)] \qquad (5)$$

where *q* represents the molecular partition function obtained as the product of the translational, q_t, rotational, q_r, and vibrational, q_v, partition functions. Due to the stoichiometry of the problem, the equilibrium constant is independent of the pressure.

Equation 5 can be simplified in the following form. In the framework of the Born−Oppenheimer approximation, the molecular partition functions in eq 5 are obtained as the product of the translational, rotational, and vibrational partition functions. In particular, for the vibrational partition function we have

$$q_\nu = \prod_i^{3N-6} \sum_{\upsilon_i=0} \exp[-\nu_i(\upsilon_i + {}^1/_2)/kT] = \prod_i^{3N-6} \frac{\exp[-\nu_i/2kT]}{1 - \exp[-\nu_i/kT]} \qquad (6)$$

Rather than using the usual closed form, the simplest treatment considers that for standard conditions only the lowest vibrational energy level is populated, and thus

$$q_\nu = \prod_i^{3N-6} \exp[-\nu_i/2kT] \qquad (7)$$

or, in terms of the zero point energy (ZPE):

$$q_\nu = \exp[-\text{ZPE}/2kT] \qquad (8)$$

This treatment is essentially that carried out by Bigeleisen and Goeppert-Mayer.[3a] Substituting eq 8 in eq 5 and using the usual semiclassical expressions for the translational and rotational partition functions,[27] we obtain

$$K = \left[\frac{m_{Py-d_5} m_{Py-H^+}}{m_{Py} m_{(Py-d_5)-H^+}}\right]^{3/2} \left[\frac{(I_a I_b I_c)_{Py} (I_a I_b I_c)_{(Py-d_5)-H^+}}{(I_a I_b I_c)_{Py-d_5} (I_a I_b I_c)_{Py-H^+}}\right]^{1/2}$$
$$\exp[(\text{ZPE}_{Py} + \text{ZPE}_{(Py-d_5)-H^+} - \text{ZPE}_{Py-H^+} - \text{ZPE}_{Py-d_5})/kT] \qquad (9)$$

In the above expression, *m* represents the molecular mass, and I_a, I_b, I_c the principal inertial moments. Equations 5 and 9 will be used and compared to determine our equilibrium constant. Equation 9 can be decomposed considering each term appearing to the right of the equal sign. Thus, we can define a translational, K_t, rotational, K_r, and vibrational, K_v, contribution to the *K* constant as

$$K_t = \left[\frac{m_{Py-d_5} m_{Py-H^+}}{m_{Py} m_{(Py-d_5)-H^+}}\right]^{3/2}$$

$$K_r = \left[\frac{(I_a I_b I_c)_{Py} (I_a I_b I_c)_{(Py-d_5)-H^+}}{(I_a I_b I_c)_{Py-d_5} (I_a I_b I_c)_{Py-H^+}}\right]^{1/2}$$

$$K_\nu = \exp[(\text{ZPE}_{Py} + \text{ZPE}_{(Py-d_5)-H^+} - \text{ZPE}_{Py-H^+} - \text{ZPE}_{Py-d_5})/kT] \qquad (10)$$

The above expressions show that K_t and K_r are independent of temperature.

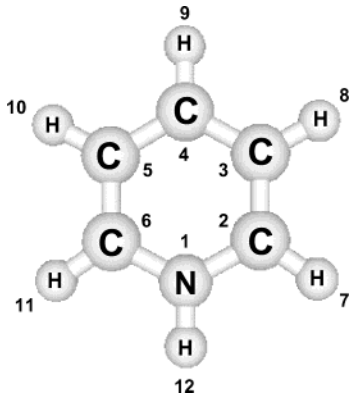

Figure 3. Numbering convention for pyridine and related ions. The figure shows the structure of the pyridinium cation obtained at the B3LYP/cc-pVTZ level.

TABLE 2: Structural Data for Pyridine (Py) and Pyridinium Cation (Py−H$^+$)[a]

	Py[b]	Py[c,d]	Py[e]	Py−H$^+$ [c]	Py-H$^+$ [f]	ρ_a[g]	ρ_a[h]
N−C2	1.338	1.333	1.340	1.347	1.337	0.351	0.326
C2−C3	1.394	1.390	1.392	1.377	1.371	0.326	0.334
C3−C4	1.392	1.388	1.391	1.393	1.390	0.325	0.324
H7−C2	1.087	1.084	1.083	1.079	1.073	0.298	0.303
H8−C3	1.083	1.081	1.081	1.079	1.072	0.294	0.300
H9−C4	1.082	1.082	1.081	1.081	1.075	0.295	0.301
H12−N				1.013	1.001		0.350
C6−N−C2	116.9	117.9	116.7	123.2	123.1		
C5−C4−C3	118.4	118.6	118.3	120.1	120.4		
C4−C3−C2	118.5	118.5	118.7	119.1	118.6		
H7−C2−N	116.0	116.1	115.9	116.8	116.8		
H8−C3−C4	121.4	121.2	120.9	121.4	117.8		
N−C4−H9	180.0	180.0	180.0	180.0	180.0		
C2−N−H12				118.4	118.5		

[a] Distances in ångstroms and angles in degrees. The table also includes the value of the electron density, ρ_a, in atomic units (e/bohr^3), at the bonded critical points. [b] Experimental data from microwave spectroscopy.[29] [c] This work, data obtained at the B3LYP/cc-pVTZ level. [d] Work of Szafran and Koput,[17] data obtained at the B3LYP/cc-pVTZ level. [e] Data obtained at the MP2/cc-pVTZ level.[17] [f] Data obtained at the RHF/6-31G(d,p) level.[30] [g] Pyridine. [h] Pyridinium cation.

Nowadays, eq 4 or 5 can be easily computed from the results of any of the available electronic structure software packages. In addition, its validity is more general than eq 9, because, depending on the fundamental frequency and the kT factor, vibrational energy levels with quantum number $\upsilon > 0$ can be populated. On the other hand, eq 9 gives a more direct insight on the mechanisms responsible for the EIE. In particular, it shows clearly the role played by the change in zero point energy. Both eqs 5 and 9 should be applied with caution when anharmonic, large amplitude vibrations do exist. The effect of these vibrations in the partition function can be, sometimes, important.[20b,28]

To compute the partition functions, the structures of pyridine and the pyridinium cation were fully optimized at the B3LYP/cc-pVTZ level. For the starting geometries, we have used the microwave experimental data for pyridine obtained by Villa el al.[29] The numbering convention is shown in Figure 3. After relaxation of the geometry we found, as expected, a planar (C_{2v}) structure for each molecule. Because the potential energy hypersurfaces are identical, the optimized structures have been used for the deuterated species. Due to the lack of structural data for pyridinium, we have collected our results in Table 2, as well as those for pyridine. These results are compared with the experimental and theoretical data found in the literature.

The optimized geometry determined for pyridine compares well with the microwave data collected in Table 2. Table 2 also shows that, with respect to pyridinium, our results exhibit longer bond distances than the previous data obtained at the Hartree−Fock (HF) level. This fact is due to the lack of correlation energy at the HF level, which is known to lead to shorter bond distances as a consequence of a too small electron repulsion.

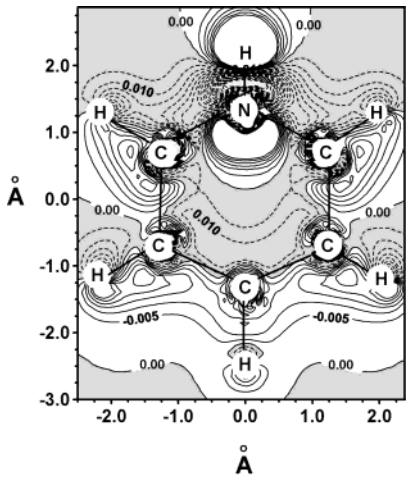

Figure 4. Electron density difference map, on the molecular plane, between pyridine and the pyridinium cation: $\Delta\rho = \rho_{Py} - \rho_{Py-H^+}$. Electron density in atomic units (e/bohr^3). Interval between isodensity lines 0.015 e/bohr^3. Data obtained from the fully optimized results. Because the nuclear positions do not match exactly in both molecules, the results around the nuclear positions must be considered semiquantitative. Positive values (shadowed zone) indicate higher electron density in pyridine, whereas negative values correspond to a higher electron density in the pyridinum cation.

Our results show that on protonation, the C2−C3 (C5−C6) and the C−H distances decrease, whereas the C3−C4 (C4−C5) and the N−C distances increase. The reason for these facts is visualized in Figure 4, which represents the electron density difference between pyridine and pyridinium ($\Delta\rho = \rho_{Py} - \rho_{Py-H^+}$) in the molecular plane. We observe a negative zone affecting the shortened bonds, i.e., higher electron density in the pyridinium cation. On the other hand, a positive difference appears in the elongated bonds, i.e., electron density is smaller in the pyridinium form.

To quantify these observations, the atoms in molecules (AIM) theory is applied to the protonated and neutral forms.[31] AIM characterizes a bond by an atomic interaction line (AIL), which is a line through the electron density, ρ, along which ρ is a maximum with respect to any neighboring line. On the AIL we found the bond critical point (BCP), a second-order saddle point where ρ reaches a minimum. The value of the electronic density at the BCP for a given bond, ρ_a, can be correlated to the concept of bond order,[31] with higher values of ρ_a corresponding to stronger bonds. Table 2 collects the ρ_a values for the different bonds found in pyridine and the pyridinium cation. We observe that on protonation the ρ_a value increases for the C2−C3 (C5−C6) and the different C−H distances, which corresponds to an increase of the bond strength. Accordingly, a decrease, corresponding to a weakening of the bond, is observed on protonation for the N−C and C3−C4 (C4−C5) bonds. Thus, protonation subtracts electron density from the N−C bonds. Therefore, the electron delocalization in pyridine is weakened.

At the equilibrium position, we obtain the rotational constants and the harmonic frequencies from a normal modes analysis. The results are collected in Table 3. The effect of deuteration is clearly reflected in the value of the frequencies. In all cases, the harmonic frequencies for the deuterated species are smaller than for the common ones. This is due to the increase of reduced

TABLE 3: Molecular Mass (amu), Rotational Constants (GHz), Harmonic Frequencies (cm^{-1}), and Zero Point Energies, ZPE (cm^{-1}), for the Protonated and Neutral Forms of Pyridine and Pyridine-d_5[a]

	Py−H$^+$	Py-d_5	Py	(Py-d_5)−H$^+$
M	80.05	84.0735	79.0422	85.0814
A	5.833	5.127	6.077	5.005
B	5.713	5.007	5.863	4.831
C	2.886	2.533	2.984	2.458
ν_1	393.5	329.1	385.5	350.1
ν_2	405.9	380.3	421.7	354.2
ν_3	624.5	538.8	617.2	530.1
ν_4	647.3	594.5	670.8	601.3
ν_5	682.7	641.2	721.6	620.4
ν_6	753.3	648.2	769.1	640.2
ν_7	859.2	700.8	900.2	693.3
ν_8	889.9	786.1	964.5	774.2
ν_9	1004.0	838.6	1011.3	834.5
ν_{10}	1019.8	838.7	1012.3	841.3
ν_{11}	1021.9	839.1	1023.6	852.9
ν_{12}	1052.9	856.4	1051.2	867.8
ν_{13}	1063.2	863.6	1079.5	876.8
ν_{14}	1082.0	908.6	1096.3	886.7
ν_{15}	1085.3	984.4	1172.9	897.5
ν_{16}	1201.4	1027.4	1243.7	984.4
ν_{17}	1228.9	1063.7	1283.2	1026.5
ν_{18}	1291.0	1274.9	1390.8	1047.7
ν_{19}	1360.0	1331.4	1476.8	1247.7
ν_{20}	1422.2	1374.1	1517.8	1351.4
ν_{21}	1524.6	1583.6	1620.9	1372.8
ν_{22}	1580.2	1584.9	1626.3	1505.3
ν_{23}	1647.2	2318.4	3142.8	1619.8
ν_{24}	1668.2	2324.9	3145.6	1620.6
ν_{25}	3201.7	2341.5	3169.4	2367.4
ν_{26}	3218.8	2356.5	3184.5	2379.8
ν_{27}	3220.4	2368.5	3192.8	2384.5
ν_{28}	3230.5			2397.1
ν_{29}	3232.0			2400.6
ν_{30}	3552.7			3552.6
ZPE	22582.60	15849.10	19446.15	18939.75

[a] The frequencies are ordered by increasing value. Data obtained at the B3LYP/cc-pVTZ level.

masses. The phenomenon is specially relevant for the five (neutral species) or six (protonated species) last frequencies, which, as determined from the normal modes composition, correspond to stretching motions of the hydrogens. The last frequency, ν_{30}, for the protonated species corresponds to the pure proton stretching, and it does not have a counterpart in the neutral form. Because the variation of the reduced mass in deuteration is small, the frequency for this mode, when going from pyridinium to pyridinium-d_5, is almost the same in both molecules.

From the data in Table 3 and using eqs 4−6, we compute $\Delta_r H^\circ_m$, $\Delta_r S^\circ_m$, and $\Delta_r G^\circ_m$ at increasing temperatures. The results are shown in Table 4. Our theoretical result for the equilibrium constant at 331 K, 0.827 ($\Delta_r G^\circ_m = +0.52$ kJ mol^{-1}), compares well with the average experimental value, 0.809 ($\Delta_r G^\circ_m = 0.58$ kJ mol^{-1}). In fact, the theoretical value is within the ± 0.027 (± 0.09 for $\Delta_r G^\circ_m$), 99.9% confidence interval of the experimental measure. These values show that in the equilibrium, the actual reaction (see Figure 1) is displaced to the left. The evolution with temperature (see Table 4) shows that the increase of temperature increases the calculated K value. The data in Table 4 also show that this effect is due to the enthalpic contributions, because of the small value of the entropic counterpart. Table 4 also collects the approximate results obtained using eq 9. In practical terms these results are equivalent to those obtained with eq 5. In particular, the K value at 331 K agrees, within the experimental confidence interval, with the value obtained from eq 5. Thus, the vibrational contribution to K, in the harmonic approach, seems to be driven by the ZPE. In addition, the independence of K_t and K_r with temperature (see eq 10) shows clearly that the variation with temperature is due solely to the vibrational contribution.

TABLE 4: Computed $\Delta_r H^\circ_m$, $\Delta_r S^\circ_m$, $\Delta_r G^\circ_m$, and K Values, at Different Temperatures, for the Proton-Transfer Reaction between Pyridine-d_5 and Pyridine[a]

	298.15 K	331 K[b]	498.15 K
$\Delta_r H^{\circ c}_m$ (kJ mol^{-1})	0.57	0.57	0.54
$\Delta_r S^{\circ c}_m$ (J mol^{-1})	0.13	0.13	0.08
$\Delta_r G^{\circ c}_m$ (kJ mol^{-1})	0.53	0.52	0.50
K^d	0.806	0.827	0.886
K^e	0.805	0.822	0.879
K^f		0.824−0.831	
K^g		0.813−0.825	

[a] $\Delta_r H^\circ_m$, $\Delta_r S^\circ_m$, and $\Delta_r G^\circ_m$ have only two significant decimal figures. The experimental value for the reaction constant at 331 K is 0.809 ± 0.027. [b] Temperature used in the experimental measurements. [c] Data obtained with eq 4. [d] Data obtained with eq 5. [e] Data obtained with eq 9. [f] Data obtained with fixed correction factors (0.99−0.95). [g] Data obtained with eq 14. Intervals [0.95−1]−[0.99−1].

TABLE 5: Translational, q_t, Rotational, q_r, and Vibrational, q_v, Contributions to the Molecular Partition Function for the Different Species Considered[a]

	Py−H$^+$	Py-d_5	Py	(Py-d_5)−H$^+$
q_t	0.2202×10^{32}	0.2370×10^{32}	0.2160×10^{32}	0.2412×10^{32}
q_r	0.5164×10^{5}	0.6295×10^{5}	0.4923×10^{5}	0.6586×10^{5}
q_v	0.4964×10^{-42}	0.3499×10^{-29}	0.3969×10^{-36}	0.5316×10^{-35}

[a] Data at 331 K.

To obtain a more detailed picture of how the change of molecular properties determines the value of the equilibrium constant, we have decomposed the molecular partition function for each molecule. The results are collected in Table 5. We can see that for the protonated forms the vibrational contribution is much smaller than for the neutral form. On the other hand, for the deuterated forms, the vibrational contributions are larger than in the neutral forms. This fact can be explained as a consequence of the higher density of states arising from the decrease in the fundamental frequencies of vibration; see Table 3. Table 5 also shows that the higher vibrational contribution is associated with pyridine-d_5, Py-d_5. This fact is a consequence of the smaller ZPE value of Py-d_5, with respect to the other molecular systems; see Table 3. With a smaller ZPE, we can expect Py-d_5 to exhibit a higher density of states. An increase of temperature will populate more vibrational states in all the compounds, resulting in an increase in all the vibrational partition functions. However, due to its higher density of states, the vibrational partition function of Py-d_5, q_{Py-d_5}, will contribute more than any other to the variation of the equilibrium constant. Because q_{Py-d_5} appears in the numerator in the expression for K (see eq 4), the increase in temperature is reflected in the increase of K.

It is of interest to consider the factors affecting the agreement between the theoretical and experimental results within the confidence interval of the measure. Thus, we apply eq 10 at 331 K. In this form, we can analyze the effect of the translational, K_t, rotational, K_r, and vibrational, K_v, contributions. From the data in Table 2, K_t and K_r are found 1.0011 and 1.0025, respectively. However, K_v amounts to 0.819. These results show that K_t and K_r predict the inverse trend for our reaction, Figure 1. K_v is the factor responsible for the correction of this trend. The present values of K_t, K_r, and K_v indicate that some or several of these contributions must change to predict the observed K

value. Equation 7 shows that the higher influence can be attributed to the vibrational contribution, due to the effect of $3N - 6$ degrees of freedom appearing in an exponential form. Even using the closed form for the harmonic vibrational partition function, eq 6, we reach the same conclusion. Thus, the vibrational contribution must be more realistically described to account for an effect as small as the SEIE in our reaction.

It is well-known that the harmonic approach leads to frequencies that are higher than the actual (anharmonic) ones. For this reason it has become customary to correct (decrease) the harmonic results obtained by electronic structure methods by a fixed amount determined by comparison with experimental data. This amount varies as a function of the level of theory and basis set used, but for the correlated level, with the B3LYP density functional, it is usually in the interval [0.99−0.95].[32] Applying correction factors of 0.99 and 0.95 to the fundamental frequencies of vibration in eq 6, we obtain K values of 0.824 and 0.831, respectively. Thus, the equilibrium constant increases from the original 0.827 value, and the difference with the average experimental result, 0.809, increases. This increase is in the direction of the confidence interval upper limit (0.836). Because the computed results are within experimental error, drawing any definitive conclusion is difficult. Anyway, it is of interest to determine the effect of a more reliable correction of the harmonic model.

Anhamonicity is translated in a set of vibrational energy levels different from those predicted by the harmonic model. In a pure stretching mode, a simple Morse oscillator shows that the density of states increases. The net result is a higher contribution to the partition function. For other anharmonic, large amplitude vibrations, such as ring puckerings or torsional motions, the pattern of energy levels has an effect on the partition function not so easily interpreted. However, this effect is small for a high-frequency mode at room temperature, because only the vibrational ground state is actually populated. The effect will be more important for low-frequency modes where the separation between levels would be not far from the kT factor. Thus, to analyze the effect of anharmonicity on K_v we need to identify the modes where only the ground state is populated.

To have an indication of the last significantly populated energy level at the temperature, T, we can follow the next line of reasoning. For a harmonic oscillator with fundamental frequency ν_0, the fraction of molecules, f_υ, in a given vibrational energy level, υ, is given by

$$f_\nu = \frac{\exp[-\nu_0 \nu/kT]}{1 - \exp[-\nu_0/kT]} \tag{11}$$

where we have used the closed form for the partition function and a Boltzmann equilibrium distribution. From eq 11 we can obtain the vibrational level, υ, with a given population, f_υ, at the T temperature as

$$\nu = -\frac{kT}{\nu_0} \ln[f_\nu(1 - \exp[-\nu_0/kT])] \tag{12}$$

Using eq 12, Figure 5 shows the correspondence between vibrational energy level, population, and ν_0 fundamental frequency, at a temperature of 331 K. The diagram shows that the limit for the $\upsilon = 1$ vibrational level to be populated less than 1% ($f_\upsilon = 0.01$) corresponds to a ν_0 fundamental frequency around 1100 cm^{-1}. At the considered temperature, vibrations with a ν_0 above that value are only significantly populated in the vibrational ground state. Thus, we can consider 1100 cm^{-1} as a practical limit to separate vibrational modes where only the ground state is populated. In other words, for these modes we will consider that the contribution to the vibrational partition function is just given by the ZPE.

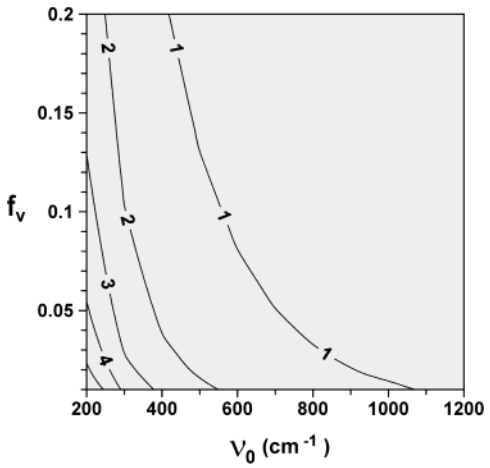

Figure 5. Graphical representation of the population of vibrational energy levels, f_v, for a given fundamental vibration frequency, ν_0, at a temperature of 331 K. The isocontour lines represent vibrational energy levels.

To analyze, at least qualitatively, the effect of anharmonicity on K_v, at 331 K, we will apply the following approach. First, the set of vibration modes is organized in two blocks, one up to 1100 cm^{-1}, and another from this limit up. Second, we compute separately the contribution of each block to the vibrational partition function. Thus, for the high-frequency modes we consider only the ZPE. On the other hand, for the low-frequency modes, we will retain the harmonic model, but due to the population of several vibrational energy levels, we will apply the closed formula, eq 6, for the vibrational partition function. In addition, the effect of anharmonicity on the density of states is especially important for the low-frequency vibrations. To include (roughly) this effect, we will apply correction factors in a given interval [x−1.0] to the low-frequency modes. Here, x is restricted to the previously considered interval of correction factors for harmonic frequencies (0.99−0.95). To represent the (a priori) decreasing density of states with the frequency, we consider the correction factor, f_i, as a function of the frequency, ν_i. Thus, expanding in a Taylor series, we have

$$f_i = \sum_n^\infty \frac{1}{n!}\left(\frac{\partial^n f_i}{\partial \nu_i^n}\right)\nu_i^n \tag{13}$$

The simplest approach is to consider up to the lineal term. Thus, $f_i = a + b\nu_i$. The a and b coefficients are obtained in each molecular species considering that $f_i = 1.0$ for $\nu_i \geq 1100$ and $f_i = x$ (lower limit of the correction factors) for the mode of lower frequency. The resulting expression for the vibrational partition function reads

$$q_\nu = \prod_i^{\text{limit}} \frac{\exp[-\nu_i f_i/2kT]}{1 - \exp[-\nu_i f_i/kT]} \prod_{j=\text{limit}+1}^{3N-6} \exp[-\nu_j/(2kT)] \tag{14}$$

where "limit" corresponds to the first vibration mode where only the ground state is populated.

Using eq 14 for q_v, we compute the equilibrium constant, K, with eq 5. We found that the K value decreases monotonically from a value of 0.825 when the correction interval is [0.99−1], to 0.813 for the interval [0.95−1]. Thus, the original 0.827 value (see Table 4) decreases, approaching the average experimental

result of 0.809. The agreement increases as the lower limit of the correction interval decreases.

Conclusions

This work presents an experimental and theoretical study of the secondary equilibrium isotope effect (SEIE) for the proton transfer between the pyridinium-d_5 cation and pyridine.The variation in bonding of pyridine, on protonation, is analyzed from the one-determinantal electron density using the atoms in molecules (AIM) theory. The results show than on protonation, electronic density is subtracted from the CN and the CC bonds further from the nitrogen. Thus these bonds are weakened, whereas the CH bonds and the CC bonds closer to the nitrogen experience an increase of electronic density and, consequently, an increase of bond strength.

The experimental results at a temperature of 331 K and high-vacuum conditions show that the actual reaction favors the neutral pyridine against the protonated pyridinium cation. The theoretical treatment predicts also this trend for the reaction. The equilibrium constant is thermostatistically computed in the rigid rotor, harmonic oscillator model. The computed value (0.827) agrees with the experimental measure (0.809) within the 99.9% confidence interval ($\pm$0.027). Analysis of the translational, rotational, and vibrational contributions to the equilibrium constant shows that the vibrational contribution is the only one responsible for the observed trend of the reaction. This fact shows that the harmonic oscillator model can yield good results for the prediction of an effect as small as the SEIE in our molecules. We also find that the reaction constant increases with the temperature; i.e., the temperature favors the formation of pyridinium cation. This fact is as a consequence of the existence of a higher density of vibrational states in the pyridine-d_5 than in the other molecular species.

We have also considered the factors affecting the agreement between the observed and experimental results. The analysis identifies the vibrational contribution as the main one responsible for discrepancies. Introduction of the usual factors in the interval [0.99−0.95], to correct the harmonic frequencies for anharmonicity, leads to increasing values of the equilibrium constant. Thus, the difference with the average observed result increases. We develop a new model that identifies the normal mode where the ground state is the only populated level. The zero point energy is only considered for the levels above this limit. For the modes below the limit, the full summation of states is applied. Here, each fundamental frequency is corrected by a factor of anharmonicity linearly dependent on the frequency value. This technique simulates an increasing density of states as the vibrational modes decrease in frequency. With the model, the computed K value approaches the experimental result. For correction factors in the interval [0.95−1], K reaches 0.815, approaching the average experimental 0.809 value. This result is the consequence of the difference between the energy levels distribution for anharmonic modes and the distribution predicted by the harmonic model. Because in the partition function the energy levels appear in an exponential form, variation in the distribution of the energy levels in low-frequency vibrations is translated into important variations of the partition function. In particular, an increase in the density of states is reflected in an increase of the partition function value. Our results show that discrepancies between the experimental and calculated K values is mainly due to the failure of the harmonic model to describe low-frequency vibrations.

Acknowledgment. This work has been supported by the "Junta de Comunidades de Castilla-La Mancha" (grant no. PAI-02-001), the "Ministerio de Ciencia y Tecnología" of Spain (grant no. BQU2000-1497), and the Universidad de Castilla-La Mancha.

References and Notes

(1) Sims, L. B.; Lewis, D. E. In *Bond Order Methods for Calculating Isotope Effects in Organic Reactions*; Isotopes in Organic Chemistry, Vol. 6; Buncel, E., Lee, C. C., Eds.; Elsevier: Amsterdam, 1984; p 161.

(2) McLennan, D. J. *In Model Calculations of Secondary Isotope Effects*; Isotopes in Organic Chemistry, Vol. 7; Buncel, E., Lee, C. C., Eds.; Elsevier: Amsterdam, 1987; p 393.

(3) (a) Bigeleisen, J.; Goeppert-Mayer, M. *J. Chem. Phys.* **1947**, *15*, 261. (b) Bigeleisen, J. *J. Chem. Phys.* **1949**, *17*, 675−678. (c) Bigeleisen. J.; Wolfsberg, M. *Adv. Chem. Phys.* **1958**, *1*, 15−76.

(4) Washburn, E. R.; Urey, H. C. *Proc. Natl. Acad. Sci.* **1932**, *18*, 496−498.

(5) (a) Stevenson, C. D.; Reidy, K. A.; Peters, S. J.; Reiter, R. C. *J. Am. Chem. Soc.* **1989**, *111*, 6578−6581. (b) Stevenson, C. D.; Sturgeon, B. E. *J. Org. Chem.* **1990**, *55*, 4090−4093. (c) Stevenson, C. D.; Halvorsen, T. D.; Reiter, R. C. *J. Am. Chem. Soc.* **1993**, *115*, 12405−12408.

(6) Hrovat, D. A.; Hammons, J. H.; Stevenson, C. D.; Borden, W. T. *J. Am. Chem. Soc.* **1997**, *119*, 9523−9526.

(7) (a) Benderskii, V. A.; Makarov, D. E.; Wight, C. A. *Chemical Dynamics at Low Temperatures*; J. Wiley & Sons: New York, 1994. (b) Grigoriev, I.; Trakhtenberg, L. I. *Processes in Solid-Phase Theory and Application;* Chemical Rubber Co.: Cleveland, OH, 1996.

(8) Kurosaki, Y.; Takayanagi, T. *J. Chem. Phys.* **1999**, *110*, 10830−10842.

(9) (a) Saueressig, G.; Bergamaschi, P.; Crowley, J. N.; Fischer, H.; Harris, G. W. *Geophys. Res. Lett.* **1995**, *22*, 1225−1228. (b) Crowley, J. N.; Saueressig, G.; Bergamaschi, P.; Fischer, H.; Harris, G. W. *Chem. Phys. Lett.* **1999**, *303*, 268−274.

(10) Laukien, F. H.; Allemann, M.; Bischofberger, P.; Grossmann, P.; Kellerhals, P.; Kopfel, P. In *Fourier Transform Mass Spectrometry, Evolution, Innovation, and Applications*; Buchanan, M. V., Ed.; ACS Symposium Series No. 359; American Chemical Society: Washington, DC, 1987; Chapter 5.

(11) (a) Abboud, J.-L. M.; Castaño, O.; Dávalos, J. Z.; Jiménez, P.; Gomperts, R.; Müller, P.; Roux, M. V. *J. Org. Chem.* **2002**, *67*, 1057−1060. (b) Abboud, J.-L. M.; Koppel, I. A.; Alkorta, I.; Della, E. W.; Müller, P.; Dávalos, J. Z.; Burk, P.; Koppel, I.; Pihl, V.; Quintanilla, E. *Angew. Chem., Int. Ed. Engl.*, **2003**, *42*, 2281−2284.

(12) Fridgen, T. D.; Keller, J. D.; McMahon, T. B. *J. Phys. Chem. A* **2001**, *105*, 3816−3824.

(13) Dunning, T. H., Jr. *J. Chem. Phys.* **1989**, *90* (2), 1007−1023.

(14) Becke, A. D. *J. Chem. Phys.* **1993**, *98*, 5648−5652.

(15) Pople, J. A.; Head-Gordon, M.; Fox, D. J.; Raghavachari, K.; Curtiss, L. A. *J. Chem. Phys.* **1989**, *90*, 5622−5629.

(16) Muñoz-Caro, C.; Niño, A.; Senent, M. L. *J. Mol. Struct. (THEOCHEM)* **2000**, *530*, 291−300.

(17) Szafran, M.; Koput, J. *J. Mol. Struct.* **2001**, *565*−*566*, 439−448.

(18) Frisch, M. J.; Trucks, G. W.; Schlegel, H. B.; Scuseria, G. E.; Robb, M. A.; Cheeseman, J. R.; Zakrzewski, V. G.; Montgomery, J. A., Jr.; Stratmann, R. E.; Burant, J. C.; Dapprich, S.; Millam, J. M.; Daniels, A. D.; Kudin, K. N.; Strain, M. C.; Farkas, O.; Tomasi, J.; Barone, V.; Cossi, M.; Cammi, R.; Mennucci, B.; Pomelli, C.; Adamo, C.; Clifford, S.; Ochterski, J.; Petersson, G. A.; Ayala, P. Y.; Cui, Q.; Morokuma, K.; Malick, D. K.; Rabuck, A. D.; Raghavachari, K.; Foresman, J. B.; Cioslowski, J.; Ortiz, J. V.; Stefanov, B. B.; Liu, G.; Liashenko, A.; Piskorz, P.; Komaromi, I.; Gomperts, R.; Martin, R. L.; Fox, D. J.; Keith, T.; Al-Laham, M. A.; Peng, C. Y.; Nanayakkara, A.; Gonzalez, C.; Challacombe, M.; Gill, P. M. W.; Johnson, B. G.; Chen, W.; Wong, M. W.; Andres, J. L.; Head-Gordon, M.; Replogle, E. S.; Pople, J. A. *Gaussian 98*, revision A.7; Gaussian, Inc.: Pittsburgh, PA, 1998.

(19) MORPHY98, a topological analysis program written by P. L. A. Popelier with a contribution from R. G. A. Bone; UMIST, Manchester, England, EU, 1998.

(20) (a) Niño, A.; Muñoz-Caro, C. *QCPE Bull.* **1997**, *17*, 1. (b) Niño, A.; Muñoz-Caro, C. *Comput. Chem.* **1997**, *21*, 143−151.

(21) See, e. g.: Marshall, A. G. *Int. J. Mass Spectrom.* **2000**, *200*, 331−357.

(22) See, e. g.: (a) Bowers, M. T.; Elleman, D. E.; King, Jr. *J. Chem. Phys.* **1969**, *50*, 1840−1845. (b) Wellman, K. M.; Victoriano, M. E.; Isolani, P. C.; Riveros, J. M. *J. Am. Chem. Soc.* **1979**, *101*, 2242−2243. (c) Jasinski, J. M.; Brauman, J. I. *J. Am. Chem. Soc.* **1980**, *102*, 2906−2912.

(23) See, e. g. (a) Wolf, J. F.; Devlin, J. L., III; Taft, R. W.; Wolfsberg, M.; Hehre, W. J. *J. Am. Chem. Soc.* **1976**, *98*, 287−289. (b) Wolf, J. F.; Devlin, J. L., III; DeFrees, D. J.; Taft, R. W.; Hehre, W. J. *J. Am. Chem. Soc.* **1976**, *98*, 5097−5101.

(24) The gas-phase basicity, GB, of a base B is defined[25] as the standard Gibbs energy change for the reaction:

$$BH^+(g) \rightarrow B(g) + H^+(g) \qquad \Delta_r G^\circ_m$$

(25) Hunter, E. P. L.; Lias, S. G. *J. Phys. Chem. Ref. Data* **1998**, *27*, 413−656.

(26) Dowdy, S.; Wearden, S. *Statistics for Research*, 2nd ed.; Wiley-Interscience: New York 1991; Chapter 8.

(27) Lucas K. *Applied Statistical Thermodynamics*; Springer-Verlag: Berlin, 1991.

(28) (a) Muñoz-Caro, C.; Niño, A. *J. Phys. Chem. A* **1997**, *101*, 4128−4135. (b) Niño, A.; Muñoz-Caro, C. *J. Phys. Chem. A* **1998**, *102*, 1177−1180. (c) Muñoz-Caro, C.; Niño, A.; Senent, M. L. *Chem. Phys. Lett.* **1997**, *273*, 135−140. (d) Torres, L.; Moreno, M.; Lluch, J. M. *J. Phys. Chem. A* **2001**, *105*, 4676−4681.

(29) Villa, E.; Amirav, A.; Lim, E. C. *J. Phys. Chem.* **1988**, *92*, 5393−5397.

(30) Nguyen, V. Q.; Tureček, F. *J. Mass Spectrom.* **1997**, *32*, 55−63.

(31) (a) Bader R. F. W. *Atoms In Molecules. A Quantum Theory*; Oxford University Press: Oxford, U.K., 1995. (b) Popelier P. *Atoms In Molecules. An Introduction*; Prentice Hall: Englewood Cliffs, NJ, 2000.

(32) Scott, A. P.; Radom, L. *J. Phys. Chem.* **1996**, *100*, 16502−16513.